Campaign Scheduling and Analysis for the Gemini Planet Imager

Dmitry Savransky[a], Bruce A. Macintosh[a], James Graham[b], Quinn M. Konopacky[c] and the GPI science team

[a]Lawrence Livermore National Lab, Livermore, CA USA [b]University of California Berkeley, Berkeley, CA USA [c]Dunlap Institute, University of Toronto, Toronto, Canada

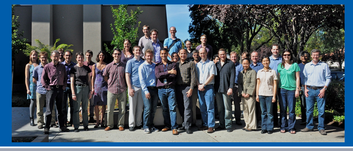

Gemini Planet Imager Exoplanet Survey (GPIES) Science

GPI is:

- An advanced, precision AO system combined with a coronagraph and integral-field, near-infrared spectrograph
- Designed to directly detect self-luminous, young, giant planets

GPIES will:

- Produce the first-ever robust census of giant planet populations in the 5-50 AU range
- Illuminate the formation pathways of Jovian planets (hot vs. cold start)
- Reveal the early dynamical evolution of planetary systems
- Provide the first examples of cool, low-gravity planetary atmospheres

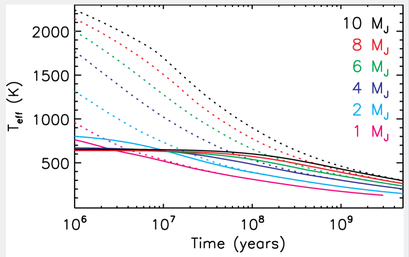

Figure 1 : Temperature of young planets assuming hot-start, or gravitational collapse (dashed), and cold-start, or core accretion (solid), formation. [Marley et al., 2007]

GPIES Deliverables:

- A catalog of exoplanets released to the Gemini community within 18 months of observation
- High-SNR GPI spectra at all 5 bands to calibrate temperature and gravity indicators for 10 planets
- Estimated effective temperatures, luminosities, and semi-major axes for all detected planets
- Empirical measurements of the number of young planets as a function of mass, semi-major axis, and stellar mass with the same precision as Doppler giant-planet surveys
- An estimated eccentricity distribution of a subset of planets
- Snapshot polarimetry images of stars predicted to have detectable debris disks
- High-SNR polarimetry images of all debris disks showing planet-induced structure
- An automated data pipeline to process images and recover calibrated astrometry and photometry
- A public catalog of all reduced images, recovered planetary properties, and detection limits

GPIES Targets

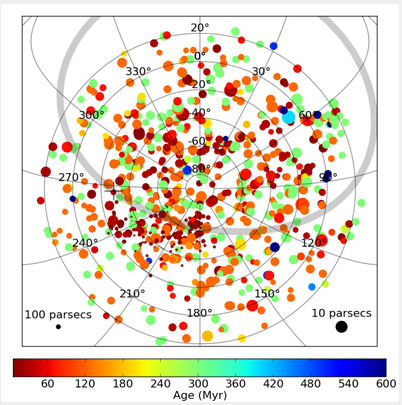

Figure 2 : GPIES targets, color coded by age and sized (inversely) by distance. The grey band represents the galactic equator with the galactic center marked by the '+'.

Type	Number in Catalog	Age (Myr)	Dist (pc)
Young FGKM	390	< 150	< 75
Older FGKM	154	< 300	< 50
Young A	82	< 300	< 75
ScoCen A	124	< 15	100 - 130
IR-Excess	32	< 600	< 75

Current target list contains 782 stars. Scheduler automatically selects the best 600 depending on when queue time is available. The final 600 targets will be selected to maximize constraints on planetary mass and semi-major-axis distributions.

Survey Simulation

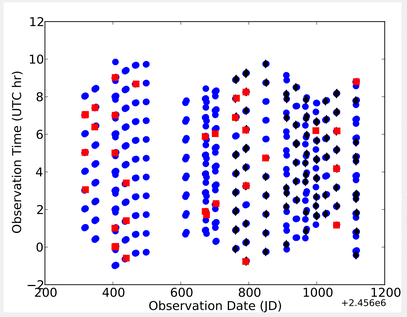

Figure 3 : Example of a survey simulation. Blue dots represent observations, red squares represent detections and black diamonds represent followup observations.

Surveys are automatically scheduled by selecting the next target which maximizes the cost function:

$$J = k_1 p_{\mathrm{det}} - k_2 \frac{t_{\mathrm{tot}}}{t_{\mathrm{rem}}}$$

where p_{det} is the probability of planetary detection [McBride et al., 2011], t_{tot} is the amount of time the target will be available for observation for the remainder of the survey, t_{rem} is the time remaining in the survey and k_1 and k_2 are normalized weights.

GPI Performance

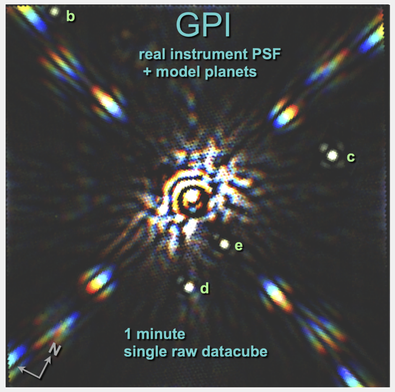

Figure 4 : Measured GPI point spread function from 1 minute observation, overlaid with modeled planet signals for HR 8799 planets [Marois et al., 2010]. Image courtesy of M. Perrin.

- GPI currently achieves raw (5σ) contrasts of 2×10^{-6} in 60 seconds in single slice of extracted H band cube.
- Spectral differential imaging generates 1×10^{-7} contrasts with 60 second exposures
- Simulated hour-long observing sequences predict 1×10^{-7} contrasts on-sky with the use of angular differential imaging (ADI).
- See Macintosh et al. [Poster 1.21] for details on current GPI performance.

GPI's measured contrast is used for all survey simulations.

Simulated Planetary Population

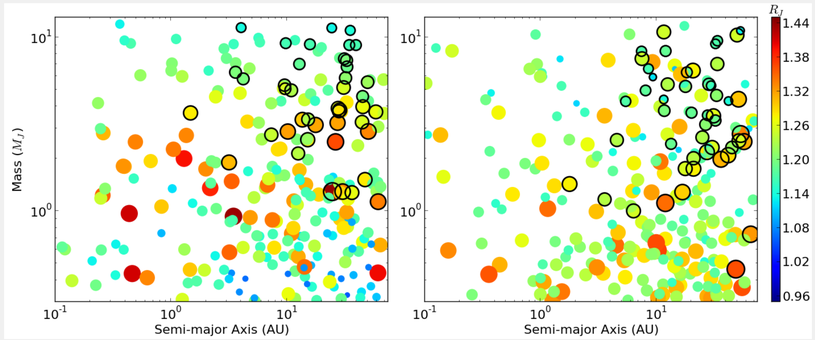

Figure 5 : Simulated population of planets based on current statistics and assuming either cold start (*left*) or hot start (*right*) model. Points with black outlines represent planets that were detected during the survey simulation. Point sizes and colors are proportional to the planet radii.

- Use Mass-Period distribution fits to known planets [Cumming et al., 2008, Howard et al., 2010] for semi-major axis distribution [McBride et al., 2011]
- Assume isotropically distributed orbital orientations - phase is sinusoidally distributed [Savransky et al., 2011]
- Calculate radii and luminosity based on formation models - i.e., Fortney et al. [2007] and Burrows et al. [2003]

Survey Completeness

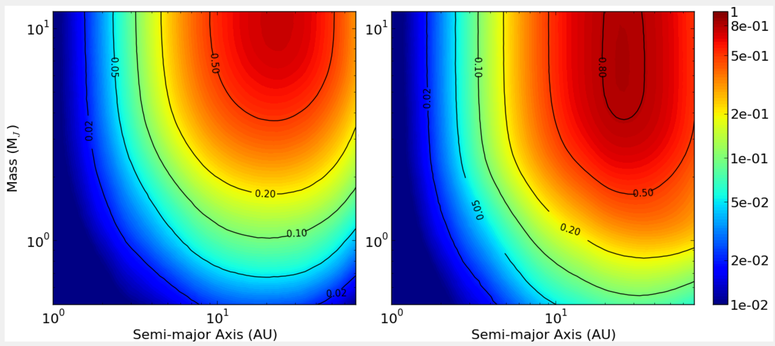

Figure 6 : The average probability per star that a planet of a given mass and semi-major axis will be discovered, assuming either cold start (*left*) or hot start (*right*) model.

Simulated Survey Results

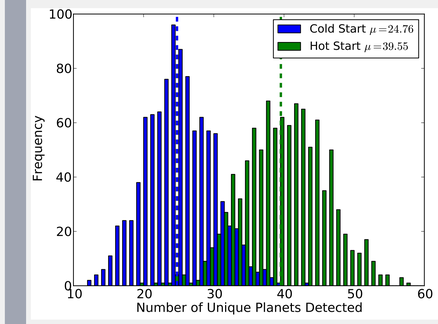

Figure 7 : Distribution of number of planets observed at least once from 1000 simulated surveys assuming cold start (blue) and hot start (green) models. In each case, the simulated planetary populations were generated to match the occurence rates from Howard et al. [2010] in each mass bin, extrapolated to all semi-major axes.

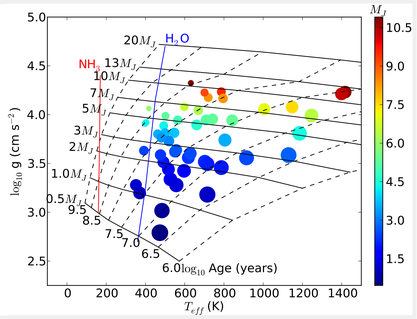

Figure 8 : Gravity vs. effective temperature showing evolutionary tracks (solid black lines) and isochrones (dashed lines) from Burrows et al. [2003]. Points are simulated planets found in one survey simulation with size proportional to the planetary radii (same scale as Figure 5) and color indicating mass. The solid red and blue lines are the approximate condensation curves for ammonia and water, respectively.

Recovered Mass and Semi-major Axis Functions

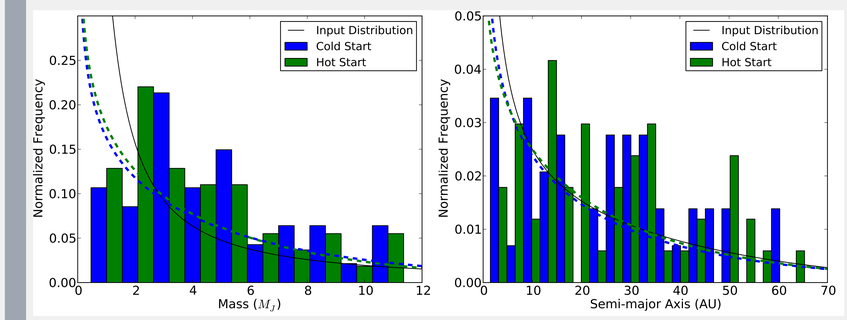

Figure 9 : Input and output distributions of mass and semi-major axis from one survey simulation assuming cold start (blue) and hot start (green) model. The dashed lines are best-fit gamma functions found via Markov chain Monte Carlo incorporating priors from Figure 6.

Eccentricity Distributions

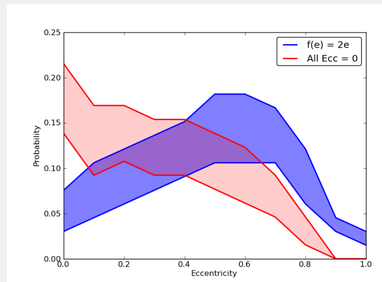

Figure 10 : Best fits for simulated population of circular (red) orbits and orbits with randomly distributed eccentricities (blue).

Based on survey simulations we can generate theoretical astrometric data points that would be obtained via multiple observations of detected planets throughout the survey. These are used to generate orbital fits via Monte Carlo methods and produce posterior distributions of eccentricity that have discriminatory power on the input distribution of planetary eccentricities.

References

A. Burrows, D. Sudarsky, and J. I. Lunine. Beyond the t dwarfs: Theoretical spectra, colors, and detectability of the coolest brown dwarfs. *The Astrophysical Journal*, 596:587, 2003.

A. Cumming, R. P. Butler, G. W. Marcy, S. S. Vogt, J. T. Wright, and D. A. Fischer. The Keck planet search: detectability and the minimum mass and orbital period distribution of extrasolar planets. *Publications of the Astronomical Society of the Pacific*, 120:531–554, 2008.

J. J. Fortney, M. S. Marley, and J. W. Barnes. Planetary radii across five orders of magnitude in mass and stellar insolation: application to transits. *The Astrophysical Journal*, 659:1661–1672, 2007.

A.W. Howard, G.W. Marcy, J.A. Johnson, D.A. Fischer, J.T. Wright, H. Isaacson, J.A. Valenti, J. Anderson, D.N.C. Lin, and S. Ida. The occurrence and mass distribution of close-in super-earths, neptunes, and jupiters. *Science*, 330(6004):653–655, 2010.

M. S. Marley, J. J. Fortney, O. Hubickyj, P. Bodenheimer, and J. J. Lissauer. On the luminosity of young jupiters. *The Astrophysical Journal*, 655(1):541, 2007.

C. Marois, B. Zuckerman, Q. M. Konopacky, B. Macintosh, and T. Barman. Images of a fourth planet orbiting HR 8799. *Nature*, 2010. ISSN 0028-0836.

J. McBride, J.R. Graham, B. Macintosh, S.V.W. Beckwith, C. Marois, L.A. Poyneer, and S.J. Wiktorowicz. Experimental design for the gemini planet imager. *Publications of the Astronomical Society of the Pacific*, 123:692–708, 2011.

D. Savransky, E. Cady, and N .J. Kasdin. Parameter distributions of keplerian orbits. *The Astrophysical Journal*, 728:66, 2011.

This work performed under the auspices of the U.S. Department of Energy by Lawrence Livermore National Laboratory under Contract DE-AC52-07NA27344. LLNL-POST-637396

savransky1@llnl.gov